

Synthesis and photoelectrochemical properties of ruthenium bisterpyridine sensitizers functionalized with a thienyl phosphonic acid moiety

Coralie Houarner-Rassin^{a,b}, Frédérique Chaignon^a, Chunxing She^c, Dave Stockwell^c,
Errol Blart^a, Pierrick Buvat^b, Tianquan Lian^{c,1}, Fabrice Odobel^{a,*}

^a *Université de Nantes, Nantes Atlantique Universités, CNRS, Faculté des Sciences et des Techniques, Laboratoire de Synthèse Organique (LSO),*

UMR CNRS 6513, 2 rue de la Houssinière, BP 92208, 44322 Nantes Cedex 3, France

^b *CEA/Le Ripault, Département Matériaux, BP16, 37260 Monts, France*

^c *Department of Chemistry, Emory University, Atlanta, GA 30322, USA*

Received 14 March 2007; received in revised form 26 April 2007; accepted 1 May 2007

Available online 5 May 2007

Abstract

We report herein the preparation, the electrochemical, the absorption and the emission properties of new heteroleptic bisterpyridine ruthenium complexes composed of a terpyridine functionalized on the 4' position by a thienyl phosphonic acid. The complexes were tested in TiO₂ dye-sensitized solar cells and were investigated by ultrafast transient IR spectroscopy on TiO₂ and SnO₂ electrodes. We found that the complex, in which the phosphonic acid group is separated by a thienyl unit to the terpyridine, displays a faster electron injection rate into the semiconductor conduction band and an improved photovoltaic photoconversion efficiency compared to the analogous complex in which the phosphonic acid group is directly linked to the terpyridine. This indicates that the thienyl unit does not restrict electron injection from the MLCT excited-state. This study highlights the benefit of introducing a thienyl unit between the phosphonic acid anchoring group and the polypyridine ruthenium sensitizer for the designing of sensitizers for solar cells and for the development of multi-molecular arrays for vectorial photoinduced electron transfer with semiconductor surface.

© 2007 Elsevier B.V. All rights reserved.

Keywords: Dye-sensitized solar cell; Ruthenium sensitizer; Solid-state solar cell; Photoelectrochemistry; Thiophene; Transient IR spectroscopy

1. Introduction

Ruthenium polypyridine complexes are valuable class of compounds that have been used in association with titanium dioxide nanoparticles for the development of dye-sensitized solar cells [1,2] but also for the designing of heteromolecular devices to achieve long-lived charge separated state [3–7]. A particularly interesting feature of the interfacial electron transfer processes involving ruthenium polypyridine complexes chemisorbed on TiO₂ surface stems from the very efficient and fast electron injection rate from the photoexcited dye and the extremely slow rate of the charge recombination reaction [8–10]. The very large ratio between the rates of the electron injection

and the back-recombination reactions, which is commonly found over three and four orders of magnitude, is an important parameter to optimize the efficiency of dye-sensitized solar cells and is also a key requirement for the designing of photochemical devices in view of long-lived charge separated states for electrocatalysis [11–13]. A promising strategy to increase the lifetime of the photogenerated ion pair (hole on the sensitizer and electron on the manifold of the TiO₂ conduction band) could be to increase the separation distance between the negative and the positive charges. Such approach could be achieved following two strategies. The first one relies on the functionalization of the sensitizer by an electron donor to shift the hole away from the TiO₂ surface and this strategy has been met with success by several teams [3–7]. The second could make use of a long “molecular wire” between the TiO₂ anchoring group and the sensitizer. In this context, ruthenium polypyridine sensitizers have been linked to TiO₂ surface through several types of linkers and rapid electron injection have been indeed observed over

* Corresponding author. Tel.: +33 2 51 12 54 29; fax: +33 2 51 12 54 02.

E-mail addresses: tlian@emory.edu (T. Lian),

Fabrice.Odobel@univ-nantes.fr (F. Odobel).

¹ Tel.: +1 404 7276649; fax: +1 404 7276586.

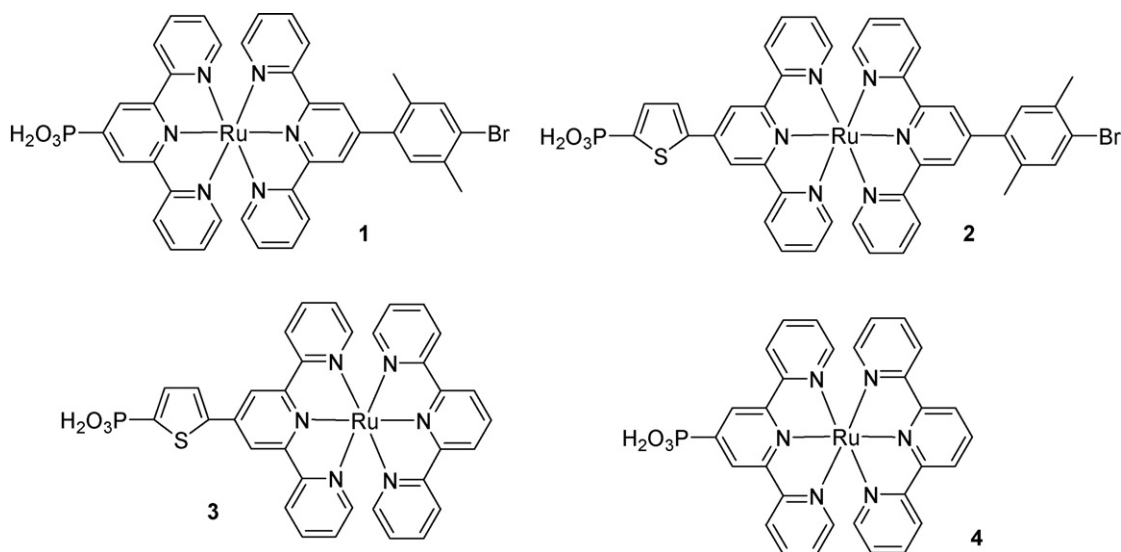


Fig. 1. Structures of the ruthenium complexes investigated in this study.

long distance [14,15]. A combination of the two latter strategies could be also envisioned in the future.

It has been shown previously that thiophene derivatives could act as a molecular wire and promote electronic interactions over large distances [16,17]. We therefore anticipate that this class of molecule could be suitable for being used as linker between TiO_2 electronic states and a ruthenium polypyridine sensitizer. Furthermore, it is known that the direct attachment of a thienyl unit to a terpyridine or a bipyridine ruthenium complex induced a bathochromic shift, an intensification of the absorptivity and an increased lifetime of the MLCT excited-state [18–20]. All these characteristics are beneficial for solar energy collection and to achieve efficient photoinduced charge separation.

We report herein the preparation and the characterisation of a new heteroleptic bis-terpyridine complex connected to TiO_2 surface through a thienyl phosphonic acid spacer (Fig. 1). In these complexes, a phosphonic acid group was preferred to the usual carboxylic acid due to the larger stability of the phosphonate linkage with TiO_2 [21,22]. The linear symmetry of the complexes **1** and **2** makes them better-suited compounds for the preparation of multi-component systems than ruthenium bipyridine complexes. In complexes **1** and **2**, an additional unit (in the place of the bromo group) could be easily introduced and will span at the opposite direction of the TiO_2 surface. This study shows the favourable impact of the thienyl unit on the charge injection reaction into the conduction band of a semiconductor.

2. Experimental

2.1. General methods

^1H and ^{13}C NMR spectra were recorded on a Bruker ARX 300 MHz Bruker spectrometer. Chemical shifts for ^1H NMR spectra are referenced relative to residual protium in the deuterated solvent (CDCl_3 , $\delta = 7.26$ ppm; MeOD , $\delta = 3.31$ ppm; CD_3CN , $\delta = 1.94$ ppm). High resolution electro-spray mass spectra (HR-ESMS) were collected in positive mode on a

MS/MS ZABSpec TOF of micromass equipped with a geometry EBE TOF. The samples were injected in mixture of $\text{CHCl}_3/\text{MeOH}$: 9/1. Electron-impact mass spectrometry (EI-MS) was recorded on a HP 5989A spectrometer.

Thin-layer chromatography (TLC) was performed on aluminum sheets precoated with Merck 5735 Kieselgel 60F₂₅₄. Column chromatography was carried out either with Merck 5735 Kieselgel 60F (0.040–0.063 mm mesh) or with SDS neutral alumina (0.05–0.2 mm mesh). Air sensitive reactions were carried out under argon in dry solvents and glassware. Chemicals were purchased from Aldrich and used as received. Compounds tetrakis(triphenylphosphine) palladium [23], 4'-diethylphosphonate-2,2':6',2''-terpyridine [21], 2,2':6',2''-terpyridine ruthenium(III) trichloride [24] and complex **4** [25] were prepared according to literature methods.

UV–vis absorption spectra were recorded on a UV-2401PC Shimadzu spectrophotometer.

The electrochemical measurements were performed with a potentiostat–galvanostat MacLab model ML160 controlled by resident software (Echem v1.5.2 for Windows) using a conventional single-compartment three-electrode cell. The working electrode was a Pt wire of 10 mm long, the auxiliary was a Pt wire and the reference electrode was the saturated potassium chloride calomel electrode (SCE). The supported electrolyte was 0.1N Bu_4NPF_6 in DMF and the solutions were purged with argon before the measurements. All potentials are quoted relative to SCE. In all the experiments the scan rate was 100 mV/s for cyclic voltammetry and 15 Hz for pulse voltammetry.

Fluorescence spectra were recorded on a SPEX Fluoromax fluorimeter and were corrected for the wavelength dependent response of the detector system.

2.2. Transient IR absorption

The transient IR absorption spectrometer was based on an amplified femtosecond Ti:sapphire laser system (coherent Vitesse oscillator, Clark-MXR CPA 1000 amplifier, 1 kHz rep-

etition rate at 800 nm, 100 fs pulse-width, 900 $\mu\text{J}/\text{pulse}$), and optical parametric and harmonic generations, which have been described in details previously [26–28]. In all the experiments presented here, a sample (of nanocrystalline thin films) was pumped at 400 nm and the subsequent absorbance change was measured in the 2000 cm^{-1} region. Transient kinetics traces at 32 probe wavelengths were collected simultaneously, from which transient spectra at different delay times were constructed. The diameters of the pump and probe beams at the samples were 400 and 300 μm , respectively. The instrument response function, i.e. the cross-correlation of the pump and probe pulses, was measured in a thin CdS film, in which 400 nm excitation led to instantaneous generation of free carriers that strongly absorbed in the mid-infrared region. The typical instrument response was well represented by a Gaussian function with a full-width-at-the-half-maximum (FWHM) of less than 200 fs.

2.3. Photoanodes preparation

TiO₂ and SnO₂ nanocrystalline thin films for transient IR absorption spectroscopy were prepared following published procedures [29–31].

For DSSCs, conductive glass substrates (F-doped SnO₂ purchased from Solaronix Co.) were cleaned with water, rinsed with acetone and ethanol and dried in a nitrogen stream. Then, transparent nanocrystalline TiO₂ films for photovoltaic measurements were prepared by doctor blading the paste purchased from Solaronix Co. (colloidal anatase Nanoxide-T, particle size of approx. 13 nm), followed by sintering at 450 °C for 30 min in air. After cooling to room temperature, the films were immersed in an approximately 3×10^{-4} M dye solution of ethanol for 16 h in room temperature. The film thickness was 3 μm .

Subsequently, a few drops of the liquid electrolyte (0.5 M of LiI, 0.05 M of I₂ and 0.1 M of 4-*tert*-butylpyridine in propylene carbonate) was inserted between the photoanode and a platinum sputtered counter-electrode.

The current–voltage characteristics of the resulting photovoltaic cell were measured by a Keithley model 2400 digital source meter with an halogen lamp calibrated to AM1.5 (air mass) intensity (1000 W m^{-2}).

2.4. Preparation of the compounds

2.4.1. 4-Bromo-2,5-dimethylbenzaldehyde 5

Two grams (7.6 mmol) of 1,4-dibromo-2,5-dimethylbenzene was dissolved in 25 mL of dry THF under argon. The solution was cooled to $-78\text{ }^{\circ}\text{C}$, then 3.4 mL (8.4 mmol) of butyllithium (2.5 M in 1-hexane) was added dropwise. The reaction mixture was stirred for 1 h, during which time 2.4 mL (68 mmol) of dry DMF was added all at once. After stirring for additional 1 h, the cooling bath was removed. The reaction solution was allowed to warm to room temperature over a 12 h period and diluted with ethyl acetate. The organic layer was washed with ammonium chloride solution and water, dried over MgSO₄, filtered and evaporated under vacuum. Purification was performed by column chromatography on silica gel with increasing gradients

of dichloromethane in petroleum ether (starting from 10/90 until 40/60) to yield **5** as a white solid (1.4 g, 83%).

¹H RMN (CDCl₃, 300 MHz): $\delta = 10.18$ (s, 1H), 7.62 (s, 1H), 7.45 (s, 1H), 2.60 (s, 3H), 2.42 (s, 3H). ¹³C RMN (CDCl₃, 75 MHz): $\delta = 192.0, 139.2, 136.1, 135.4, 133.5, 133.0, 131.3, 22.2, 18.4$. MS (EI): m/z (%) = 213 (84), 211 (100), 183 (34), 104 (43).

2.4.2. 4'-(4-Bromo-2,5-dimethylphenyl)-2,2',6',2''-terpyridine 6

2-Acetylpyridine (0.57 g, 4.7 mmol) was added dropwise to a solution of potassium *tert*-butoxide (0.8 g, 7 mmol) in 30 mL of dry THF. The reaction mixture was stirred under argon for 30 min to give a cream-white suspension. 0.53 g (2.3 mmol) of 4-bromo-2,5-dimethylbenzaldehyde in 5 mL of dry THF was then added dropwise. The solution was stirred overnight at room temperature and then 1.8 g (23 mmol) of ammonium acetate in 15 mL of ethanol/acetic acid (2/1) was added. The mixture was heated to reflux for 6 h. The reaction mixture was cooled to room temperature, poured onto ice and water (100 g) to give a pale yellow precipitate that was collected by filtration and dried. The filtrate was extracted with dichloromethane. The organic layer was dried over MgSO₄, filtered and evaporated under vacuum to give a brown oil. This crude product and the yellow precipitate were purified by column chromatography on alumina with increasing gradients of ethyl acetate in petroleum ether (starting from 0/100 until 30/70) to yield **6** as a white solid (0.50 g, 48%).

¹H RMN (CDCl₃, 300 MHz): $\delta = 8.70$ (d, ³J = 3.9 Hz, 2H), 8.67 (d, ³J = 7.8 Hz, 2H), 8.42 (s, 2H), 7.88 (ddd, ⁴J = 1.2 Hz, ³J = 7.8 Hz, ³J = 7.8 Hz, 2H), 7.48 (s, 1H), 7.34 (ddd, ⁴J = 1 Hz, ³J = 4.8 Hz, ³J = 7.8 Hz, 2H), 7.24 (s, 1H), 2.40 (s, 3H), 2.31 (s, 3H). ¹³C RMN (CDCl₃, 75 MHz): $\delta = 156.1, 155.4, 150.9, 149.2, 138.8, 136.8, 135.3, 134.5, 133.9, 131.6, 123.8, 121.3, 22.2, 19.7$. MS (EI): m/z (%) = 416 (84, ⁸¹M⁺), 414 (100, ⁷⁹M⁺).

2.4.3. 4'-(2-Bromo-5-thienyl)-2,2',6',2''-terpyridine 8

2-Acetylpyridine (0.67 g, 5.5 mmol) was added dropwise to a solution of potassium *tert*-butoxide (0.9 g, 8.3 mmol) in 40 mL of dry THF. The reaction mixture was stirred under argon for 30 min to give a cream-white suspension. 0.53 g (2.7 mmol) of 2-bromothiophene carboxaldehyde in 10 mL of dry THF was then added dropwise. The solution was stirred overnight at room temperature and then 2.1 g (27 mmol) of ammonium acetate in 20 mL of ethanol/acetic acid (2/1) was added. The mixture was heated to reflux for 6 h. The reaction mixture was cooled to room temperature, poured onto ice and water (150 g) to give a pale yellow precipitate that was collected by filtration and dried. The filtrate was extracted with dichloromethane. The organic layer was dried over MgSO₄, filtered and evaporated under vacuum to give a brown oil. This crude product and the yellow precipitate were purified by column chromatography on alumina with increasing gradients of ethyl acetate in petroleum ether with triethylamine (starting from 0/98/2 until 30/68/2) to yield **8** as a white solid (0.53 g, 53%).

¹H NMR (CDCl₃, 300 MHz): $\delta = 8.72$ (d, ³J = 4.8 Hz, 2H), 8.62 (d, ³J = 7.8 Hz, 2H), 8.58 (s, 2H), 7.87 (ddd, ⁴J = 1.8 Hz, ³J = 7.5 Hz, ³J = 7.5 Hz, 2H), 7.51 (d, ³J = 3.9 Hz,

1H), 7.35 (ddd, $^4J = 1$ Hz, $^3J = 4.8$ Hz, $^3J = 7.8$ Hz, 2H), 7.11 (d, $^3J = 3.9$ Hz, 1H). ^{13}C NMR (CDCl_3 , 75 MHz): $\delta = 156.2, 155.8, 149.1, 143.3, 142.5, 136.8, 131.2, 128.3, 127.1, 125.9, 124.0, 121.3, 117.1, 116.6, 114.2$. MS (EI): m/z (%) = 395 (37), 314 (100).

2.4.4. 4'-(2-Diethylphosphonate-5-thienyl)-2,2',6',2''-terpyridine **9**

A sealed tube was charged with 100 mg (0.25 mmol) of 4'-(2-bromo-5-thienyl)-2,2',6',2''-terpyridine and 330 mg (1.27 mmol) of triphenylphosphine in 7 mL of dry toluene. The mixture was degassed by pumping and flushing with argon on the vacuum line and then 55 mg (0.51 mmol) of triethylamine, 32 mg (0.027 mmol) of tetrakis(triphenylphosphine) palladium and 100 mg (0.76 mmol) of diethylphosphite was added. The mixture was heated to 120 °C for 14 h. After cooling to room temperature, the solvent was evaporated under vacuum. Purification was performed by column chromatography on alumina with increasing gradients of ethyl acetate in petroleum ether to yield **9** as a white solid (80 mg, 72%).

^1H NMR (CDCl_3 , 300 MHz): $\delta = 8.70$ (d, $^3J = 4.8$ Hz, 2H), 8.68 (s, 2H), 8.60 (d, $^3J = 7.8$ Hz, 2H), 7.84 (ddd, $^4J = 1.5$ Hz, $^3J = 7.8$ Hz, $^3J = 7.8$ Hz, 2H), 7.75 (t, $^3J = 3.6$ Hz, 1H), 7.68 (dd, $^3J = 3.6$ Hz, $^3J = 8.1$ Hz, 1H), 7.34 (ddd, $^4J = 1.2$ Hz, $^3J = 4.8$ Hz, $^3J = 7.8$ Hz, 2H), 4.17 (m, 4H), 1.35 (t, 6H). ^{13}C NMR (CDCl_3 , 75 MHz): $\delta = 156.3, 155.6, 149.2, 142.1, 136.9, 133.2, 129.6, 126.44, 124.1, 121.3, 117.4, 62.1, 16.3$. MS (EI): m/z (%) = 451 (96), 315 (100).

2.4.5. 4'-(4-Bromo-2,5-dimethylphenyl)-2,2',6',2''-terpyridine ruthenium(III) trichloride **10**

A mixture of $\text{RuCl}_3 \cdot 3\text{H}_2\text{O}$ (60 mg, 0.28 mmol) and 4'-(4-bromo-2,5-dimethylphenyl)-2,2',6',2''-terpyridine **6** (100 mg, 0.24 mmol) in EtOH (7 mL) was heated to reflux for 5 h. The reaction mixture was cooled and the brown solid that formed was collected by filtration. The crude product **10** was washed with diethyl ether, dried and used without further purification (138 mg, 92%).

2.4.6. 4'-Diethylphosphonate-2,2':6',2''-terpyridine-(4'-(4-bromo-2,5-dimethylphenyl)-2,2':6',2''-terpyridine) ruthenium(II) di-tetrafluoroborate **12**

A suspension of 4'-(4-bromo-2,5-dimethylphenyl)-2,2':6',2''-terpyridine ruthenium(III) trichloride **10** (54 mg, 0.12 mmol) and AgBF_4 (114 mg, 0.58 mmol) was heated to 60 °C for 2 h in acetone (20 mL). After cooling to room temperature, the solution was filtered to remove AgCl and the filtrate was placed in a round bottom flask with *n*-butanol (10 mL). Acetone was evaporated under vacuum and the solution was degassed. 40 mg (0.09 mmol) of 4'-diethylphosphonate-2,2':6',2''-terpyridine was added and the resulting mixture was refluxed for 3 h. After cooling to room temperature, the desired complex was precipitated by addition of petroleum ether. The suspension was filtered and dried under vacuum. The crude product was purified by column chromatography on silica gel, eluted with pure acetone and then with increasing gradients

of water and saturated KNO_3 solution in acetone (starting from acetone/ $\text{H}_2\text{O}/\text{KNO}_3$ 90:10:0, until 79:20:1), to give a red product. The solid was dissolved in methanol and treated with NaBF_4 solution to precipitate **12** as a red solid (36 mg, 40%).

^1H NMR (CD_3CN , 300 MHz): $\delta = 8.95$ (d, $^3J = 13.5$ Hz, 2H), 8.74 (s, 2H), 8.68 (d, $^3J = 8.1$ Hz, 2H), 8.52 (d, $^3J = 8.1$ Hz, 2H), 7.95 (m, 4H), 7.78 (s, 1H), 7.64 (s, 1H), 7.48 (d, $^3J = 5.4$ Hz, 2H), 7.32 (d, $^3J = 5.4$ Hz, 2H), 7.20 (m, 2H), 7.15 (m, 2H), 4.20 (m, 4H), 2.62 (s, 3H), 2.54 (s, 3H), 1.51 (t, 6H). HRMS-ESI (m/z): calcd for $[\text{C}_{42}\text{H}_{38}\text{B}_2\text{BrF}_8\text{N}_6\text{O}_3\text{PRu}]^{2+}$ 443.0485; found 443.0490.

2.4.7. 4'-(2-Diethylphosphonate-5-thienyl)-2,2':6',2''-terpyridine-[4'-(4-bromo-2,5-dimethylphenyl)-2,2':6',2''-terpyridine] ruthenium(II) di-tetrafluoroborate **13**

A suspension of 4'-(4-bromo-2,5-dimethylphenyl)-2,2':6',2''-terpyridine ruthenium(III) trichloride **10** (71 mg, 0.11 mmol) and AgBF_4 (57 mg, 0.29 mmol) was heated to 60 °C for 2 h in acetone (20 mL). After cooling to room temperature, the solution was filtered to remove AgCl and the filtrate was placed in a round bottom flask with *n*-butanol (10 mL). Acetone was evaporated under vacuum and the solution was degassed. Forty milligrams (0.09 mmol) of 4'-(2-diethylphosphonate-5-thienyl)-2,2',6',2''-terpyridine **9** was added and the resulting mixture was refluxed for 3 h. After cooling to room temperature, the desired complex was precipitated by addition of petroleum ether. The suspension was filtered and dried under vacuum. The crude product was purified by column chromatography on silica gel, eluted with pure acetone and then with increasing gradients of water and saturated KNO_3 solution in acetone (starting from acetone/ $\text{H}_2\text{O}/\text{KNO}_3$ 90:10:0, until 79:20:1), to give a red product. The solid was dissolved in methanol and treated with NaBF_4 solution to precipitate **13** as a red solid (40 mg, 50%).

^1H NMR (CD_3CN , 300 MHz): $\delta = 8.98$ (s, 2H), 8.74 (s, 2H), 8.68 (d, $^3J = 8.1$ Hz, 2H), 8.52 (d, $^3J = 7.8$ Hz, 2H), 8.23 (t, $^3J = 3.6$ Hz, 1H), 7.95 (ddd, $^4J = 18$ Hz, $^3J = 7.5$ Hz, $^3J = 7.5$ Hz, 4H), 7.85 (dd, $^3J = 3.6$ Hz, $^3J = 8.1$ Hz, 1H), 7.78 (s, 1H), 7.64 (s, 1H), 7.46 (d, $^3J = 5.4$ Hz, 2H), 7.42 (d, $^3J = 5.2$ Hz, 2H), 7.20 (m, 4H), 4.20 (m, 4H), 2.54 (s, 3H), 2.47 (s, 3H), 1.36 (t, 6H). HRMS-ESI (m/z): calcd for $[\text{C}_{46}\text{H}_{40}\text{BrN}_6\text{O}_3\text{PRuS}]^{2+}$ 484.0423; found 484.0400.

2.5. General procedure for the hydrolysis of the diethyl phosphonate ester in the complexes

To a solution of the previous complex **12** or **13** in freshly distilled DMF was carefully added an excess of dry trimethylsilylbromide under argon. The mixture was heated at 50 °C for 36 h under argon. After cooling to room temperature, the desired complex was precipitated by addition of NaBF_4 solution. The suspension was filtered, washed with NaBF_4 solution and dried under vacuum. The solid was dissolved in methanol and treated with two drops of trifluoromethane sulfonic acid to precipitate a red solid. Then, the complex was purified by column chromatography using Sephadex LH 20 as stationary phase and acetonitrile as eluent.

2.5.1. 4'-Phosphonic acid-2,2':6',2''-terpyridine-(4'-bromo-2,5-dimethylphenyl)-2,2':6',2''-terpyridine ruthenium(II) di-tetrafluoroborate **1**

Prepared according to the general procedure described below but using **12** (70 mg, 0.05 mmol) and dry trimethylsilylbromide (400 mg, 2.5 mmol) in 5 mL of DMF. Yield: 80%. ¹H NMR (MeOD, 300 MHz): δ (ppm) 9.11 (d, ³J = 13.5 Hz, 2H), 8.97 (s, 2H), 8.75 (m, 2H), 8.01 (m, 4H), 7.76 (s, 1H), 7.69 (s, 1H), 7.58 (d, ³J = 5.4 Hz, 2H), 7.48 (d, ³J = 5.4 Hz, 2H), 7.20 (m, 4H), 2.62 (s, 3H), 2.54 (s, 3H).

2.5.2. 4'-(2-Phosphonic acid-5-thienyl)-2,2':6',2''-terpyridine-[4'-bromo-2,5-dimethylphenyl)-2,2':6',2''-terpyridine] ruthenium(II) di-tetrafluoroborate **2**

Prepared according to the general procedure described below but using **13** (20 mg, 0.02 mmol) and dry trimethylsilylbromide (96 mg, 0.6 mmol) in 3 mL of DMF. Yield: 80%. ¹H NMR (MeOD, 300 MHz): δ (ppm) 9.00 (s, 2H), 8.74 (s, 2H), 8.70 (d, ³J = 8.1 Hz, 2H), 8.52 (d, ³J = 7.8 Hz, 2H), 8.13 (t, ³J = 3.6 Hz, 1H), 7.95 (m, 4H), 7.78 (s, 1H), 7.63 (s, 1H), 7.62 (m, 1H), 7.46 (d, ³J = 4.8 Hz, 2H), 7.43 (d, ³J = 5.4 Hz, 2H), 7.19 (m, 4H), 2.62 (s, 3H), 2.55 (s, 3H). HRMS-ESI (*m/z*): calcd for [C₄₂H₃₂BrN₆O₅PRuS]²⁺ 456.0110; found 456.0099.

2.5.3. 4'-(2-Phosphonic acid-5-thienyl)-2,2':6',2''-terpyridine-2,2':6',2''-terpyridine ruthenium(II) di-tetrafluoroborate **3**

First, the heteroleptic diethylester complex was prepared according to the procedure described for **13** using terpyridine ruthenium trichloride (54 mg, 0.12 mmol), AgBF₄ (114 mg, 0.58 mmol) followed by the addition of the ligand **9** (80 mg, 0.17 mmol). Yield 75%. ¹H NMR (CD₃CN, 300 MHz): δ (ppm) 8.96 (s, 2H), 8.74 (d, ³J = 8.1 Hz, 2H), 8.68 (d, ³J = 8.1 Hz, 2H), 8.50 (d, ³J = 7.8 Hz, 2H), 8.43 (t, ³J = 8.1 Hz, 1H), 8.28 (t, ³J = 3.6 Hz, 1H), 7.93 (ddd, ⁴J = 1.8 Hz, ³J = 7.5 Hz, ³J = 7.5 Hz,

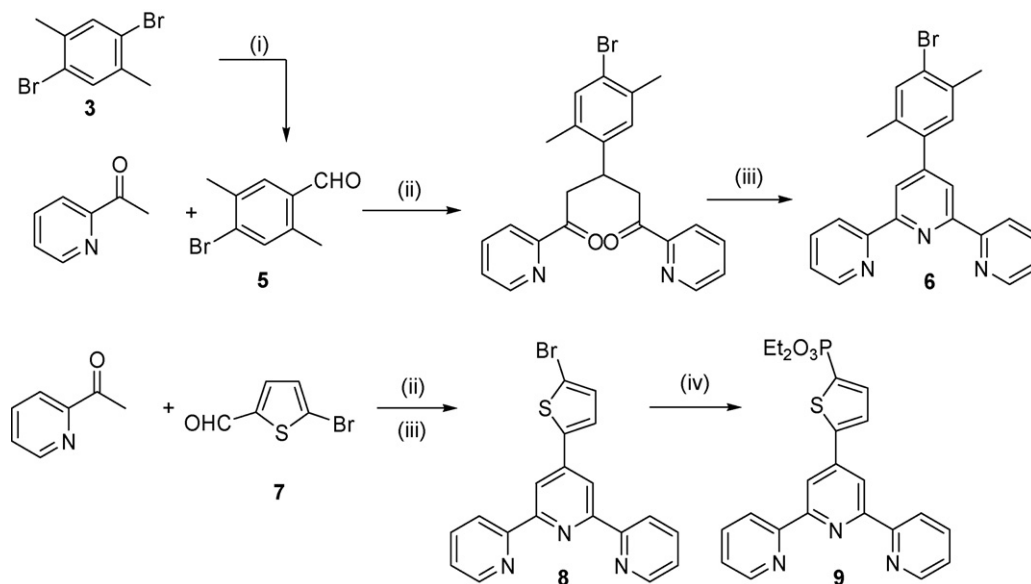
4H), 7.84 (dd, ³J = 3.6 Hz, ³J = 8.1 Hz, 1H), 7.42 (d, ⁴J = 5.7 Hz, 2H), 7.36 (d, ³J = 5.7 Hz, 2H), 7.17 (m, 4H), 4.21 (m, 4H), 1.37 (t, 6H). HRMS-ESI (*m/z*): calcd for [C₃₈H₃₃N₆O₃PruS]²⁺ 393.0558; found 393.0500.

The latter complex (15 mg, 0.015 mmol) was hydrolysed according to the general procedure described above using trimethylsilylbromide (82 mg, 0.5 mmol) in 3 mL of DMF. Yield: 80%. ¹H NMR (MeOD, 300 MHz): 8.98 (s, 2H, H₂), 8.74 (d, ³J = 8.1 Hz, 2H), 8.68 (d, ³J = 8.1 Hz, 2H), 8.52 (d, ³J = 7.8 Hz, 2H), 8.43 (t, ³J' = 8.1 Hz, 1H), 8.24 (t, ³J = 3.6 Hz, 1H), 7.95 (ddd, ⁴J = 1.8 Hz, ³J = 7.5 Hz, ³J = 7.5 Hz, 4H), 7.85 (dd, ³J = 3.6 Hz, ³J = 8.1 Hz, 1H), 7.41 (d, ³J = 5.4 Hz, 2H), 7.36 (d, ³J = 5.2 Hz, 2H), 7.18 (m, 4H).

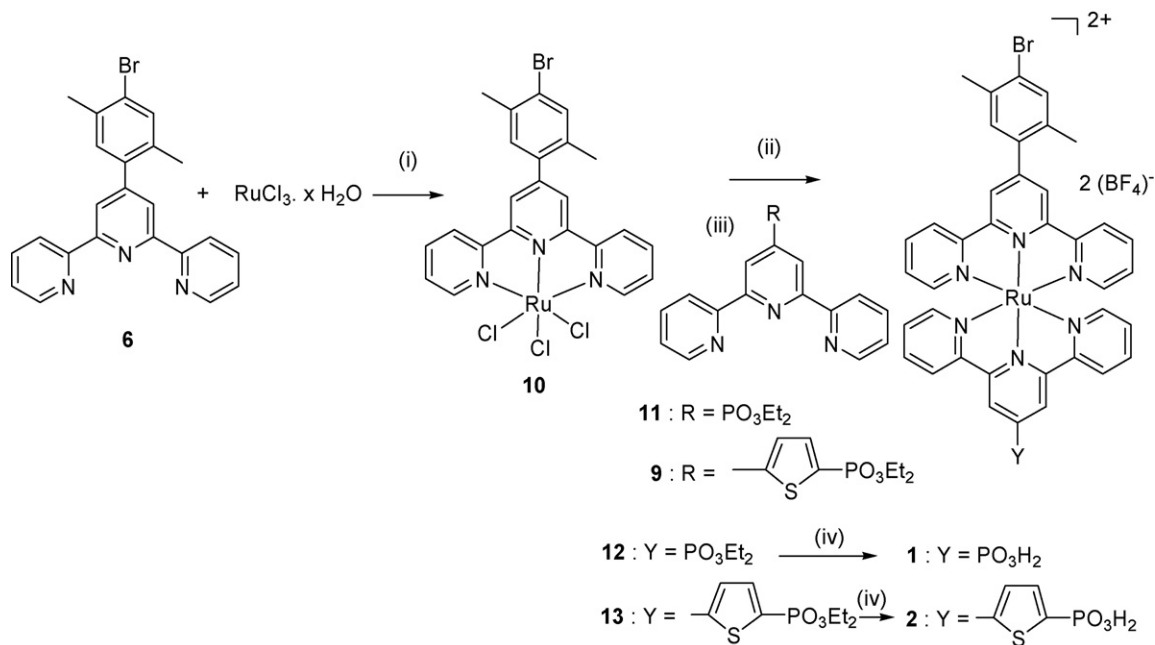
3. Results and discussion

3.1. Synthesis of the ligands

The synthesis of the new terpyridyl ligands **6** and **9** is shown in Scheme 1. The preparation of **6** was achieved according to a Kröhnke methodology [32] and it required the bromodimethyl benzaldehyde **5**. Lithiation of the commercially available dibromodimethyl benzene with butyllithium at -78 °C followed by treatment with DMF afforded **5** in 65% yield. The resulting bromo dimethyl benzaldehyde **5** was then reacted with 2 equiv. of acetylpyridine to form the intermediate diketone. The latter was not isolated, but directly cyclized with ammonium acetate to give the corresponding dihydropyridine, which undergoes oxidation into the desired terpyridine **6** with a 48% isolated yield. Following a similar two-step procedure, bromothiophenyl terpyridine **9** was synthesized in a 53% yield from bromo thiophene carbaldehyde **7** [33]. The phosphonate ester group was subsequently introduced on **8** by a palladium cross-coupling reaction with diethylphosphite following the conditions previously published for polypyridine derivatives [34].



Scheme 1. Synthetic routes for the preparation of the terpyridyl ligands **6** and **9**. Reagents and conditions: (i) (1) BuLi, THF, -78 °C, 1 h; (2) DMF, -78 °C, 1 h (83%); (ii) *t*BuOK, THF, RT, 16 h; (iii) NH₄OAc, EtOH/H₂O, reflux, 6 h (48%); (iv) HPO₃Et₂, PPh₃, Et₃N, Pd(PPh₃)₄, toluene, 120 °C, 14 h (72%).



Scheme 2. Preparation of the heteroleptic bisterpyridine ruthenium complexes (i) EtOH, reflux, 5 h (92%); (ii) AgBF₄, acetone, 60 °C, 2 h; (iii) ligand **9** or **11** addition in *n*-BuOH, reflux, 3 h (50%); (iv) Me₃SiBr, DMF, 50 °C, 36 h then aqueous sol. of NaBF₄ (80%).

3.2. Preparation of the ruthenium complexes

The preparation of the heteroleptic ruthenium complexes with terpyridyl ligands **6**, **9** or **11** is outlined in Scheme 2. Bromo dimethyl phenyl terpyridine **6** was first metallated by 1 equiv. of ruthenium trichloride in ethanol affording the insoluble dark brown complex **10**. The chloro ligands were subsequently removed with silver tetrafluoroborate and the second terpyridyl ligand was introduced. The two complexes **12** and **13** were thus obtained in about 50% yield after purification by column chromatography. Finally, the diethyl phosphonate group in **12** and **13** was hydrolyzed in mild conditions using trimethylsilyl bromide in DMF. To examine the effect of the dimethyl bromophenyl substituent on the terpyridine, the ruthenium bisterpyridine complex **3** was also synthesized according to the same strategy, but start-

ing from the known terpyridine ruthenium trichloride and the ligand **9**. It is noteworthy that the remaining bromo group in complexes **1** and **2**, could be used to introduce a supplementary functional unit such as an oxidation redox catalyst [11] or an electron donor [3–7].

3.3. UV–vis electronic absorption spectroscopy

The complexes were first characterized by UV–vis spectroscopy. The spectra of **1–4** are shown in Fig. 2 and their spectroscopic characteristics are collected in Table 1.

The spectra of the complexes **1–4** feature intense absorption bands in the UV region (250–320 nm) attributed to π – π^* ligand-centered transitions. The broad absorption band in the visible region corresponds to well-known spin-allowed metal-to-ligand

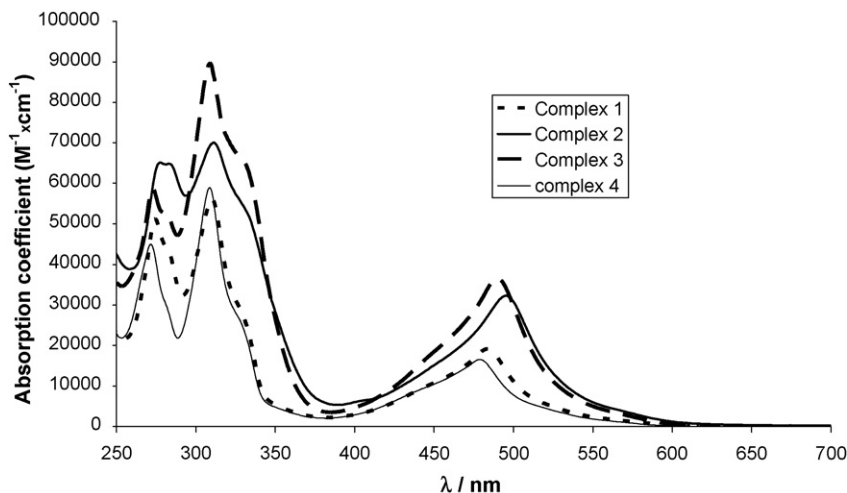


Fig. 2. Absorption spectra of the complexes **1–4** recorded in acetonitrile.

Table 1
Spectroscopic characteristics of the complexes **1–4**

Complex	Absorption ^a λ_{\max} (nm) ($\epsilon/M^{-1} \text{ cm}^{-1}$)	Emission		E_{00} (³ MLCT) ^b (eV)
		λ_{em} at RT ^a	λ_{em} at 77 K ^c	
1	485 (19,600)	640	611	2.03
2	492 (32,300)	686	656	1.89
3	490 (34,400)	685	658	1.88
4	482 (16,400)	638	616	2.01

^a Recorded at room temperature in acetonitrile.

^b E_{00} was determined from the maximum emission wavelength in the phosphorescent spectrum at 77 K.

^c Recorded at 77 K in ethanol.

charge-transfer (MLCT) transition centered around 490 nm. The maximum absorbance of the MLCT transition of the complexes **2** and **3** is significantly shifted to longer wavelengths compared to the complexes **1** and **4** (Fig. 2 and Table 1). This is a direct consequence of the stabilization of the LUMO orbital of the terpyridyl ligand substituted by the thienyl phosphonic acid substituent (see below). Furthermore, the presence of the thienyl spacer also enhances considerably the molar absorption coefficient of the MLCT transition; most probably due to the larger transition dipole moment arising from the longer distance of the charge shift (from the HOMO $d\pi\text{Ru}$ orbital to the LUMO π^* extended thienyl terpyridine orbital). On the other hand, the dimethyl bromophenyl substituent on the adjacent terpyridine has a minor influence on the MLCT transition, since the absorption and emission maximum wavelengths of **1** and **2** is very close to that of **4** and **3**, respectively (Fig. 2 and Table 1).

3.4. Electrochemical study

The prepared complexes **1–4** were studied by cyclic voltammetry and exhibit quasi-reversible oxidation and reduction processes (Table 2). It is well-established that in ruthenium(II) polypyridine complexes the oxidation is metal-centered, while the reduction is ligand-centered. As expected, the first oxidation potential of all the complexes is almost identical within the series. This is consistent with the involvement of a $d\pi(t_2g)$ ruthenium orbital, which is only slightly affected by the substituents on the terpyridine ligands.

In the cathodic region, the easiest ligand to be reduced is that substituted by a thienyl (complexes **2** and **3**). By comparison with other studies, it is clear that in the complexes **2** and **3**, the first reduction process ($E_{1/2} = -1.1$ V versus SCE) involves the addition of an electron in the terpyridine substituted by the

thienyl fragment. It is interesting to note that the terpyridine directly substituted by the phosphonic acid group (**1** and **4**) displays higher lying LUMO orbital by ca. 140 meV compared to the terpyridine substituted by a thienyl phosphonic acid (**2** and **3**). This indicates that the thienyl moiety induces a stabilization of the LUMO orbital in the anchoring terpyridyl ligand probably due to the extension of the π -conjugated system. The second reductive process corresponds to electron injection in the adjacent terpyridine ($E_{1/2} = -1.43$ V versus SCE) which concerns the dimethyl bromophenyl terpyridine in **1** and **2** or the unsubstituted terpyridine in complexes **3** and **4**.

3.5. Steady-state emission spectroscopy

The luminescence spectra of the complexes were recorded at room temperature in acetonitrile and at 77 K in ethanol glass and the results are gathered in Table 1. Steady-state emission spectra of the series of complexes **1–4** are shown in Fig. 3. At 77 K and at room temperature the emission maximum of the MLCT phosphorescence is ranked in the order: **1** \approx **4** \ll **3** \approx **2**, which is consistent with the observed trend in the absorption spectra. This indicates that the complexes **2** and **3** exhibit a lower triplet excited-state than complexes **1** and **4** owing to the stabilization of the LUMO orbital of the terpyridine substituted with the thienyl phosphonic acid unit. As a result, complexes **2** and **3** exhibit probably more delocalized triplet MLCT excited-state than **1** and **4** corresponding to an electron localized on the thienyl terpyridine anchored to TiO_2 surface. Furthermore, we also notice that the dimethyl bromo benzene substituent imparts little electronic perturbation of the MLCT excited-state since the absorption and the emission characteristics of **2** and **3** or **1** and **4** are very similar (Fig. 1 and Table 1). Most probably the two methyl groups on the phenyl creates steric hindrance that prevents flatness of the phenyl with the central pyridine, limiting the π -conjugation between these two fragments.

3.6. Photoelectrochemical properties

In order to evaluate the influence of the thiophene unit on the electron injection efficiency of these complexes, the photocurrent–voltage characteristics (I – V) of sandwich-type photovoltaic cells were recorded with a nanocrystalline TiO_2 electrodes (Table 3). The well-known N_3 sensitizer ($\text{N}_3 = \text{Ru}(\text{dcbpy})_2\text{NCS}_2$ with $\text{dcbpy} = 4,4'$ -dicarboxylic acid-2,2'-bipyridine) was also used as a benchmark reference.

As expected, the overall efficiency of the complexes **1–4** are much lower than that of N_3 due to the lower absorbance of the

Table 2
Electrochemical data of the complexes **1–4** recorded in DMF with 0.1 M Bu_4NPF_6 as supporting electrolyte

Complex	$E_{1/2}(\text{Ru}^{\text{III}}/\text{Ru}^{\text{II}})$ (V)	$E_{1/2}(\text{terpy}0/-1)$ (V)	$E_{1/2}(\text{terpy}0/-1)$ (V)	$E_{1/2}(\text{Ru}^{\text{III}}/*\text{Ru}^{\text{II}})$ (V)
1	1.32	–1.26	–1.43	–0.71
2	1.32	–1.10	–1.43	–0.57
3	1.33	–1.10	–1.43	–0.55
4	1.32	–1.22		–0.69

All potentials are referred to saturated calomel electrode (SCE). $E_{1/2}(\text{Ru}^{\text{III}}/*\text{Ru}^{\text{II}}) = E_{1/2}(\text{Ru}^{\text{III}}/\text{Ru}^{\text{II}}) - E_{00}(\text{³MLCT})$.

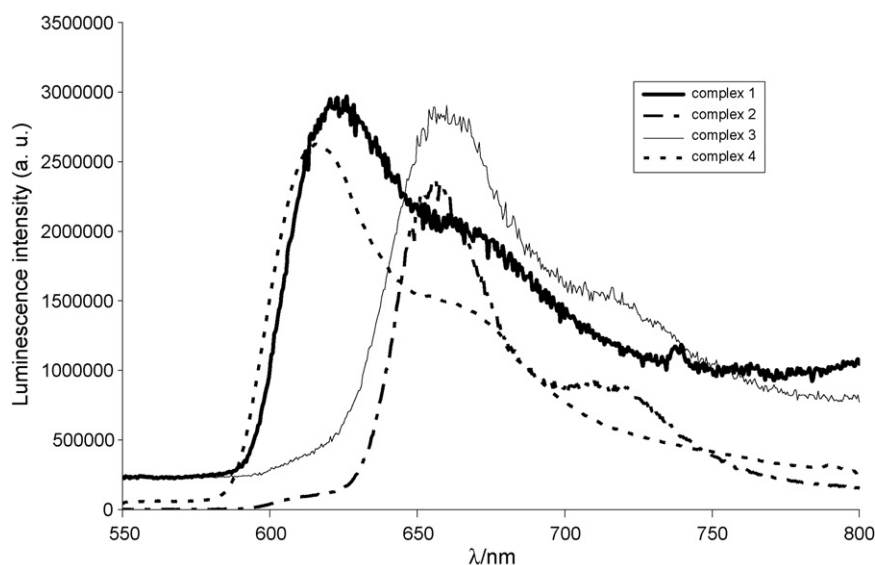


Fig. 3. Emission spectra of the complexes **1–4** recorded in glass ethanol at 77 K.

ruthenium bisterpyridine complexes in the red part of the solar spectrum and a lower injection quantum yield compared to N₃ (*vide infra*). Although quite low, the photoconversion efficiencies of these complexes are still higher than those reported for other ruthenium bisterpyridine complexes [35].

Within this series of complexes, the best overall photoconversion efficiency is obtained with the complexes **2** and **3**, which contain the thienyl spacer between the terpyridine and the phosphonic acid anchoring group. If we take into account that the electron injection driving force for the complexes **1** and **4** is larger than for **2** and **3**, this result indicates that the electrons certainly tunnels efficiently through the thienyl unit (Table 2). The higher overall photoconversion efficiency of complexes **2** and **3** comes from a slightly higher open-circuit photovoltage and a substantial higher short-circuit photocurrent compared to complexes **1** and **4**. In complexes **2** and **3**, the red-shifted MLCT absorption band and the faster injection rate explain the higher photocurrent. The photopotential delivered by a solar cell is proportional to the flux of the injected electrons in the semiconductor, but it decreases with the electron recombination reaction occurring between the injected electrons with the oxidized sensitizers [36]. The higher photovoltage measured with complexes **2** and **3** could be accounted by a slower rate of the

back-recombination reaction with the oxidized sensitizer owing to a larger distance with the TiO₂ surface [37].

3.7. Transient absorption studies

To gain some insight of how the thienyl unit affects the solar cell performance, the electron injection kinetics from dyes **3** and **4** were measured. These two dyes differ only by the presence or the absence of the thienyl unit between the phosphonate and the terpyridine. Complexes **1** and **4** are similar to **2** and **3**, except they lack the dimethyl bromophenyl substituent on one terpyridine. Fig. 4 shows a comparison of the injection kinetics traces from dyes **3**, **4** and N₃. The kinetics traces were measured by exciting the sensitizer at 400 nm and probing the change of injected electron absorption in $\sim 1965\text{--}1985\text{ cm}^{-1}$ [26,38,39]. These traces have been scaled (by the absorption at 400 nm) to correspond to the same number of absorbed excitation photons; therefore the amplitudes of the signal represent the relative electron injection yields. Absorption from the blank film, similar in amplitude to those in dyes **3** and **4** sensitized film, have been subtracted from these traces. As shown in Fig. 4, the IR signal of dyes **3** and **4** rises within the instrument response time and shows a slight decay in the 1 ns window. The rise time of the IR absorption signal is estimated to be <100 fs, similar to the fast component observed in N₃ sensitized film under the same condition. However, the amplitude of the signal is significantly smaller than that of N₃ sensitized film. It was shown previously, in N₃/TiO₂, the electron kinetics is biphasic consisting of a <100 fs component and slower components on the ps and longer time scale [39]. The <100 fs injection component can be attributed to injection from unrelaxed excited-state producing hot electrons high above the conduction band edge, whose relaxation of the hot electron gave rises to the observed decay in the IR probe signal [26,27,38,39]. The decays in dyes **3** and **4** sensitized TiO₂ film, as shown in Fig. 4, can also be attributed to the same origin. The much smaller signal amplitude in these dyes suggests that the rate of injection

Table 3

Photoelectrochemical data of the sensitizers **1–4** along with that of N₃ collected under simulated AM 1.5 solar light (1000 W/m²)

Complex	i_{SC} (mA/cm ²)	V_{OC} (V)	ff (%)	Overall efficiency (%)
1	1.0	0.46	60	0.28
2	1.23	0.57	70	0.50
3	1.14	0.52	70	0.41
4	0.55	0.42	74	0.17
N ₃	12.0	0.72	47	4.00

V_{OC} : open-circuit voltage; i_{SC} : short-circuit current; ff: filling factor. The electrolyte was solution of propylene carbonate containing 0.5 M of LiI, 0.05 M of I₂ and 0.1 M of 4-*tert*-butylpyridine.

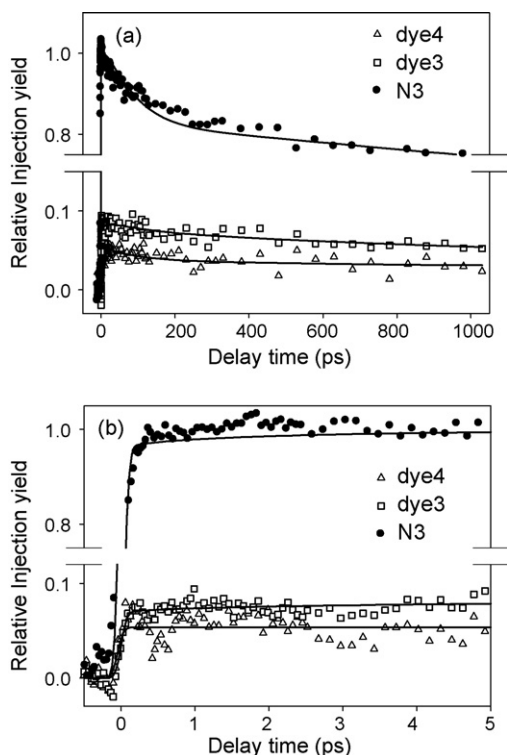


Fig. 4. Electron injection kinetics to TiO_2 from N3, dyes **3** and **4**. The kinetics traces were measured at $1965\text{--}1985\text{ cm}^{-1}$ after 400 nm excitation of sensitized films that are exposed to air. The signal amplitudes have been scaled to correspond to the same number of excited molecules and reflect the relative electron injection yield.

from the unrelaxed state was significantly slowed down in these complexes compared to N3. Most excited molecules relax to the vibronically relaxed $^3\text{MLCT}$ states, from which electron injection is either too slow to be observed in the 1 ns window or is thermodynamically prohibited. The latter can be attributed to the low excited-state potential in these terpyridine complexes.

It is interesting to note that the relative initial signal size in films sensitized by dyes **3**, **4** and N3 is, respectively, 10%, 15% and 1, which is similar to the ratio of overall solar cell conversion efficiency in dyes **3**, **4** and N3 (Table 3). However, a direct comparison of these quantities is difficult as the latter depends on many other quantities in addition to the injection yield. Furthermore, the transient IR measurement is conducted in films that are exposed to air, whose conduction band edge position is likely different from those in the working solar cells. The latter is in an electrolyte solution of propylene carbonate containing lithium cation and 4-*tert*-butyl-pyridine, that certainly affects the conduction band energy at the electrolyte–electrode interface.

The higher signal amplitude in dye **3** than dye **4** sensitized TiO_2 suggested that the thienyl unit did not reduce the electronic coupling strength to TiO_2 in the former complex. Unfortunately, the small amplitude/injection yield in TiO_2 hindered a more careful analysis of the role of thienyl unit. To further investigate its effect, the injection kinetics from dyes **3**, **4** and N3 in SnO_2 films (exposed to air) were compared (Fig. 5). These kinetics traces were measured by exciting the sensitizer at 400 nm and probing the change of injected electron absorp-

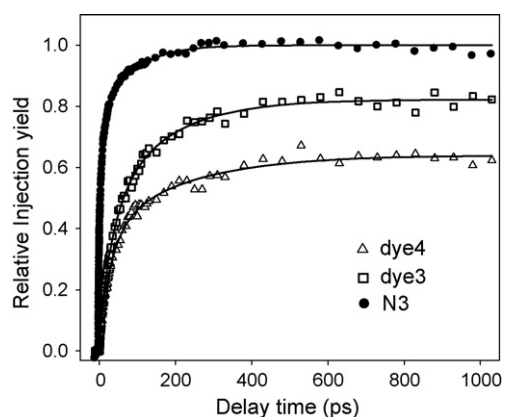


Fig. 5. Comparison of electron injection kinetics to SnO_2 film from dyes **3**, **4** and N3. The kinetics traces were recorded by probing the injected electron absorption at $1900\text{--}1940\text{ cm}^{-1}$ after 400 nm excitation. The signal amplitudes have been scaled to correspond to the same number of excited molecules and reflect relative electron injection yield.

tion in $\sim 1900\text{--}1940\text{ cm}^{-1}$ [26,38,39]. These traces have been scaled by the number of absorbed excitation photons and the amplitudes of the signal represent the relative electron injection yields. Absorption from the blank film is much smaller in amplitude than the sensitized films and have been subtracted from these traces. The injection kinetics are multiexponential in all samples. The kinetics of N3 to SnO_2 is similar to previous published results [40], consisting of a $\sim 10\%$ < 100 fs injection component and slow components on the ps time scale. The kinetics can be roughly characterized by a half-rise time, defined as the time of 50% injection yield, of ~ 5 ps. The half rise times of injection from dyes **3** and **4** are 65 and 150 ps, respectively. The faster injection rate of dye **3** relative to dye **4** in spite of the lower driving force (Table 2) of the former complex clearly suggests that the thienyl unit enhances the electronic coupling from the terpyridine to SnO_2 .

The electron injection yield of dyes **3** and **4** at 1 ns are about 80 and 60% of that of N3. The injection process appears to be incomplete and continue to grow beyond 1 ns. These yields are much larger than those measured on TiO_2 , and can be attributed to the 0.5 V lower conduction band edge position in SnO_2 . The conduction band edge position of SnO_2 and TiO_2 are indeed estimated at, respectively, -0.3 and -0.8 V (versus SCE) at pH 7 making thus the electron injection reaction from the relaxed $^3\text{MLCT}$ states of dyes **3** and **4** energetically allowed. These results suggest that the 4'-phosphonic acid thienyl terpyridine ligand can be a viable anchoring group to semiconductors if the $^3\text{MLCT}$ excited-state is sufficiently reducing by using suitable ligands in the rest of the coordination sphere of the ruthenium.

4. Conclusions

The preparations of three new terpyridine ligands functionalized by a thienyl phosphonic acid or dimethyl bromo phenyl terpyridine substituents and the corresponding ruthenium complexes are reported. The introduction of a thiophene unit between the phosphonic acid anchoring group and the terpyridine induces a stabilization of the MLCT excited-state of the complex owing

to a decrease of the energy level of the LUMO orbital of the terpyridine ligand.

The new complexes were tested as sensitizers in TiO₂ sandwich photovoltaic cells and we demonstrated that the thienyl spacer does not restrict the photovoltaic performances of the sensitizer, since it even improves substantially the overall photoconversion efficiency. The IR transient spectroscopy study also indicates that the injection rate through the thienyl unit is not decreased compared to the terpyridine directly functionalized with the phosphonic acid group. Therefore, thiophene and possibly oligothiophene spacers could be suitable molecular wires to promote remote electron injection from ruthenium sensitizers into the semiconductor conduction band. Although the overall photoconversion efficiency of the two complexes is quite low compared to the best sensitizers due to the too low injection driving force, however, the 4'-phosphonic acid thienyl terpyridine ligand represents a promising molecular basis for the design of new ruthenium sensitizers and new dyads equipped with electron donors to generate long-lived charge separated state. The replacement of the second terpyridine by more electron releasing ligands such as thiocyanato or electron-rich polypyridine ligands would probably increase the light harvesting efficiency of the complex and lower its oxidation potential and would thereby most probably improve the photovoltaic performances of the complex [41]. The potential valuable properties of these new complexes are the longer separation distance to TiO₂ surface and the linear symmetry of these rigid molecules, which is favourable to control the organization of a linear molecular array attached on semiconductor surface [42].

Acknowledgements

Commissariat à l'Énergie Atomique (CEA) and Région Pays de la Loire are gratefully acknowledged for the salary of CH and Ministère de la Recherche for the program "ACI Jeune Chercheur" for the salary of FC. T.L. also acknowledges the financial support by US DOE, Office of Science (grant no. DE-FG02-98ER14918).

References

- [1] A. Hagfeldt, M. Grätzel, *Acc. Chem. Res.* 33 (2000) 269–277.
- [2] K. Kalyanasundaram, M. Grätzel, *Coord. Chem. Rev.* 77 (1998) 347–414.
- [3] R. Argazzi, N.Y. Murakami Iha, H. Zabri, F. Odobel, C.A. Bignozzi, *Coord. Chem. Rev.* 248 (2004) 1299–1316.
- [4] N. Robertson, *Angew. Chem. Int. Ed.* 45 (2006) 2338–2345.
- [5] N. Hirata, J.-J. Lagref, E.J. Palomares, J.R. Durrant, M.K. Nazeeruddin, M. Grätzel, D.D. Censo, *Chem. Eur. J.* 10 (2004) 595–602.
- [6] S.A. Haque, S. Handa, K. Peter, E. Palomares, M. Telakkat, J.R. Durrant, *Angew. Chem. Int. Ed.* 44 (2005) 5740–5744.
- [7] P. Bonhôte, J.-E. Moser, R. Humphry-Baker, N. Vlachopoulos, S.M. Zakeeruddin, L. Walder, M. Grätzel, *J. Am. Chem. Soc.* 121 (1999) 1324–1336.
- [8] B. Wenger, M. Grätzel, J.-E. Moser, *J. Am. Chem. Soc.* 127 (2005) 12150–12151.
- [9] S.Y. Huang, G. Schlichthoerl, A.J. Nozik, M. Grätzel, A.J. Frank, *J. Phys. Chem. B* 101 (1997) 2576–2582.
- [10] S.A. Haque, Y. Tachibana, R.L. Willis, J.E. Moser, M. Grätzel, D.R. Klug, J.R. Durrant, *J. Phys. Chem. B* 104 (2000) 538–547.
- [11] J.A. Treadway, J.A. Moss, T.J. Meyer, *Inorg. Chem.* 38 (1999) 4386–4387.
- [12] R.W. Murray (Ed.), *Molecular Design of Electrode Surfaces*, vol. 22, John Wiley, New York, 1992.
- [13] M.S. Wrighton, *Science* 231 (1986) 32–37.
- [14] P. Piotrowiak, E. Galoppini, Q. Wei, G.J. Meyer, P. Wiewior, *J. Am. Chem. Soc.* 125 (2003) 5278–5279.
- [15] E. Galoppini, W. Guo, W. Zhang, P.G. Hoertz, P. Qu, G.J. Meyer, *J. Am. Chem. Soc.* 124 (2002) 7801–7811.
- [16] R. Ziessel, *Synthesis* (1999) 1839–1865.
- [17] F. Odobel, S. Suresh, E. Blart, Y. Nicolas, J.P. Quintard, P. Janvier, J.-Y. Le Questel, B. Illien, D. Rondeau, P. Richomme, T. Häupl, S. Wallin, L. Hammarström, *Chem. Eur. J.* 8 (2002) 3027–3046.
- [18] S. Encinas, L. Flamigni, F. Barigelletti, E.C. Constable, C.E. Housecroft, E.R. Schofield, E. Figgemeier, D. Fenske, M. Neuburger, J.G. Vos, M. Zehnder, *Chem. Eur. J.* 8 (2002) 137–150.
- [19] A. Barbieri, B. Ventura, L. Flamigni, F. Barigelletti, G. Fuhrmann, P. Bauerle, S. Goeb, R. Ziessel, *Inorg. Chem.* 44 (2005) 8033–8043.
- [20] R. Ziessel, P. Bäuerle, M. Ammann, A. Barbieri, F. Barigelletti, *Chem. Commun.* (2005) 802–804.
- [21] S.M. Zakeeruddin, M.K. Nazeeruddin, P. Pechy, F.P. Rotzinger, R. Humphry-Baker, K. Kalyanasundaram, M. Grätzel, *Inorg. Chem.* 36 (1997) 5937–5946.
- [22] I. Gillaizeau-Gauthier, F. Odobel, M. Alebbi, R. Argazzi, E. Costa, C.A. Bignozzi, P. QuD. Meissner, *Inorg. Chem.* 40 (2001) 6073–6079.
- [23] M. Schlosser, *Organometallics in Synthesis: A Manual*, John Wiley, Chichester, 1994.
- [24] C.A. Bessel, R.A. Leising, L.F. Szczipura, W.J. Perez, M.H. Vo Huyhn, K.J. Takeuchi, *Inorg. Synth.* 32 (1998) 186–198.
- [25] C. Houarner-Rassin, E. Blart, P. Buvat, F. Odobel, *J. Photochem. Photobiol. A: Chem.* 186 (2007) 135–142.
- [26] J.B. Asbury, E. Hao, Y. Wang, H.N. Ghosh, T. Lian, *J. Phys. Chem. B* 105 (2001) 4545–4557.
- [27] J.B. Asbury, N.A. Anderson, E. Hao, X. Ai, T. Lian, *J. Phys. Chem. B* 107 (2003) 7376–7386.
- [28] Y. Wang, J.B. Asbury, T. Lian, *J. Phys. Chem. A* 104 (2000) 4291–4299.
- [29] T. Nutz, U.Z. Felde, M. Haase, *J. Chem. Phys.* 110 (1999) 12142–12150.
- [30] A. Zaban, S. Ferrere, J. Sprague, B.A. Gregg, *J. Phys. Chem. B* 101 (1997) 55–57.
- [31] C. She, N.A. Anderson, J. Guo, F. Liu, W.-H. Goh, D.-T. Chen, D.L. Mohler, Z.-Q. Tian, J.T. Hupp, T. Lian, *J. Phys. Chem. B* 109 (2005) 19345–19355.
- [32] F. Kröhnke, *Synthesis* (1976) 1–24.
- [33] E. Figgemeier, V. Aranyos, E.C. Constable, R.W. Handel, C.E. Housecroft, C. Risinger, A. Hagfeldt, E. Mukhtar, *Inorg. Chem. Commun.* 7 (2004) 117–121.
- [34] V. Penicaud, F. Odobel, B. Bujoli, *Tetrahedron Lett.* 39 (1998) 3689–3692.
- [35] K. Kilsa, E.I. Mayo, D. Kuciauskas, R. Villahermosa, N.S. Lewis, J.R. Winkler, H.B. Gray, *J. Phys. Chem. A* 107 (2003) 3379–3383.
- [36] A. Hagfeldt, M. Grätzel, *Chem. Rev.* 95 (1995) 49–68.
- [37] J.N. Clifford, E. Palomares, M.K. Nazeeruddin, M. Grätzel, J. Nelson, X. Li, N.J. Long, J.R. Durrant, *J. Am. Chem. Soc.* 126 (2004) 5225–5233.
- [38] N.A. Anderson, T. Lian, *Coord. Chem. Rev.* 248 (2004) 1231–1246.
- [39] N.A. Anderson, T. Lian, *Annu. Rev. Phys. Chem.* 56 (2005) 491–519.
- [40] X. Ai, N.A. Anderson, J. Guo, T. Lian, *J. Phys. Chem. B* 109 (2005) 7088–7094.
- [41] M.K. Nazeeruddin, P. Pechy, T. Renouard, S.M. Zakeeruddin, R. Humphry-Baker, P. Comte, P. Liska, L. Cevey, E. Costa, V. Shklover, L. Spiccia, G.B. Deacon, C.A. Bignozzi, M. Grätzel, *J. Am. Chem. Soc.* 123 (2001) 1613–1624.
- [42] H. Imahori, *J. Mater. Chem.* 17 (2007) 31–41.